A control approach for fast voice coil actuators for servo valve applications in mobile and industrial hydraulics

Lucian Năşcuţiu*, Olivier Reinertz** and Hubertus Murrenhoff**

Technical University of Cluj-Napoca, Faculty of Mechanics, Mechanical Engineering Department,
Muncii str. 103-105, 400641 Cluj-Napoca, Romania*
RWTH Aachen University, Institute for Fluid Power Drives and Systems (IFAS),
Campus Boulevard 30, D-52074 Aachen, Germany**
E-Mail: Lucian.Nascutiu@termo.utcluj.ro

The resonant behaviour of voice coil actuators driven by fast changing signals limits their application in hydraulic servo valves. A very good damping, precision and the ability to dynamically overcome the effects of flow forces are some special requirements. The paper attempts to propose some control strategies and solutions to reduce the effects of raising impedance near the resonant frequency, thus improving the damping, which allows further enhancements in bandwidth. Theoretical models and simulation results are presented and discussed and some recommendations are proposed. The parameters used in simulation correspond to those of an already developed and tested voice coil prototype.

Keywords: voice coil actuators, direct operated servo valves, fast switching valves, impedance, robust control
Target audience: Industrial and Mobile Hydraulics, Hydraulic Components, Process Control

1 Introduction

The nowadays research focuses on the issues that arise in specific servo hydraulic applications in power generation, building safety (smart buildings, smart structures, mobile bridges), materials testing, automotive and aerospace engineering, and astronomy (intelligent telescope mirror control) as well as in manufacturing technology. New technological advances require an increase in speed and accuracy, while at the same time augmenting demands for safety, energy saving, efficiency and for environmental compatibility arise. This applies especially for applications in the field of industrial and mobile hydraulics. The requirements for precision and high dynamics in hydraulic drive systems can be accomplished by introducing intelligent fluid devices that operate at low power levels and can handle very high power with high efficiency. A special category of such fluid devices is represented by proportional valves and servo valves /1/, /2/. They are nowadays, mostly microprocessor based mechatronic devices. To further increase their performances, some researchers have proposed original solutions, by improving also the internal valve's mechanical structure. An example is the roto-translating valve, which presents a secondary rotary type actuator connected to a sleeve interposed between the spool and the valve body, thus composing a roto-translating valve. Due to its structure, the metering control precision and valve speed are virtually quadratic in respect to the traditional spool position control /3/, /4/.Another technological advance in the field refers to high performance valve actuators /1/, /5/, /6/, /7/, /8/, /9/. The voice coil motors are here representative. They show a high level of accuracy and high acceleration, making them a very good candidate in the valve technology field. Nowadays, a special application of the voice coil motors lies in the field of digital hydraulics /5/. This area is particularly of high interest to increase the efficiency in wind power plants, where the mechanical transmissions are to be replaced with hydraulic transmissions /5/, /10/. In this case the electrical generator is directly driven at rated speed, which corresponds to a 50 Hz frequency of the grid. The digital hydraulic machines are discretely-adjustable variable displacement units (pumps or motors) having a number of independent controllable cylinder-piston pairs. The total flow rate sink or sourced of those machines varies stepwise, like the binary representation of the numbers in digital systems. A number of cylinder-piston pairs (usually 5,7 or 9), driven simultaneously by a slow rotating camshaft, can be dynamically enabled, disabled or idled by using fast switching valves (for example for 7 pairs the flow rate can take 2^7=128 discrete values). They are driven by voice coil motors, in PWM mode or continuous mode, to adjust the flow rate at the required level. For a pump or a motor operating at 50 Hz (20 ms period), in order to achieve a 10% pulse width, the valves must be switched in 2 ms! A very well damping behaviour is required for these valves, in order to prevent very high pressure peaks and high amount of heat losses. The switching technology in fluid power systems leads to very small throttling losses and therefore to high efficiency.

A voice coil motor, designed for direct operated hydraulic servo valves must fulfil some special requirements. A very good damping behaviour, very high developed force, the ability to quickly overcome the effects of the flow forces and a very precise positioning capability of the valve's spool are some conditions to achieve a very good stationary and transient behaviour as well as a good efficiency of the driven system. An earlier work of the authors proposes to investigate new alternatives of electro-mechanical drives to replace the still expensive special (piezo and magnetostrictive) materials /1/, or sensitive structures (torque motors) while at the same time improving the stationary and transient behaviour according to the new technological advances. The authors have developed a highly dynamic and very precise valve actuator prototype /8/, based on the voice coil principle. Its properties and performances are shortly presented in the following.

2 Properties and performance of the first prototype

A novel geometry of the magnetic circuit and the arrangement of the coil windings inside the voice coil actuator allows to reduce the electrical time constant, thus supporting a high dynamics. The coil geometry consists of three groups of windings (series connected). Each two adjacent groups are wounded in opposite direction; therefore the mutual inductance is negative. Moreover, double of this mutual inductance is subtracted from the sum of self-inductances. This arrangement yields therefore an overall lower inductance for the same wire resistance, compared to a coil with the same number of turns wounded in the same direction.

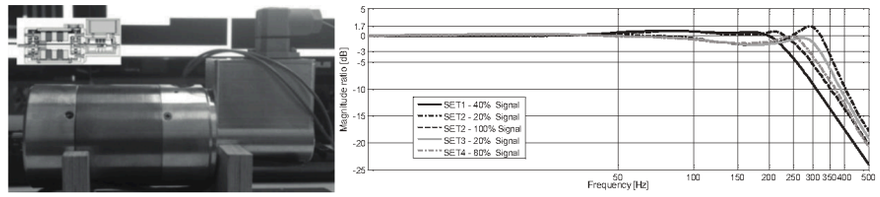

Figure 1: The IFAS prototype (left) and the experimental Bode plot (right)/8/

The properties of the test assembly and the prototype are summarised in the following tables:

Supply voltage	36 V
Maximal supply current	3.6 A
Coil excursion	±1.2 mm
DC coil resistance at 20 °C	7.2 Ω
Mechanical natural frequency	176 Hz
Movable mass	70 g

Force factor k_F	29 N/A
Back-emf constant	28.8 V s/m
Electrical time constant	0.388 ms
Maximal force	104 N
LVDT gain	4.45 V/mm
Current sensor gain	1.6 V/A

Table 1: The prototype parameters /8/.

The actuator was tested without a real load (i.e. a servo valve). To simulate a real damping, the gaps of the magnetic circuit were filled with a small amount of mineral oil based ferro fluid, thus increasing the viscous friction on both sides of the coil /11/. The curves of the Bode plot corresponds to the actuator with ferro fluid inserted in the gaps, except the SET1.The -3dB frequency of the responses lies between 270 Hz and 350 Hz, depending on the controllers' parameters.

3 The mathematical model of the voice coil motor

3.1 The linear model

The mathematical model of the actuator /8/, /9/, /12/, /13/ is mainly composed of two linear differential equations corresponding to both the electric and the mechanical part:

$$\begin{cases} u = R_e \cdot i + L_e \cdot \dfrac{di}{dt} + k_{emf} \cdot \dot{x} \\ k_F \cdot i = m \cdot \ddot{x} + c_D \cdot \dot{x} + k_E \cdot x + F_D \end{cases} \quad (1)$$

The coefficientk_F, represents the motor force sensitivity or force factor, k_{emf} the back-emf constant ($k_{emf} \approx k_F$), R_e the DC resistance of the coil, L_e the inductance of the coil, u the effective voltage applied to the coil, m the total moving mass, c_D the damping coefficient, k_E the total suspension stiffness, i the current through the coil and$x$ the coil position. The force F_D takes into account all disturbances seen from the load side.

3.2 The impedance model of the voice coil motor

The impedance model of the voice coil motor can be derived from the equation system 1, by dividing the second equation by the force sensitivity k_F and considering the variable i (the coil current), the output variable /8/. With the variable u (the coil voltage supply) as input, the complex impedance is then calculated as $Z_0(j\omega) = U(j\omega)/I(j\omega)$, which is actually the inverse of the transfer function.The following notations are adopted:

$$C_m = \frac{m}{k_F \cdot k_{emf}}, R_m = \frac{k_F \cdot k_{emf}}{c_D}, L_m = \frac{k_F \cdot k_{emf}}{k_E} \quad (2)$$

whereC_m, R_m and L_m are virtually electric quantities, which represent the influence of the mechanical system on the overall actuator behaviour. They are called the "mechanical" capacity, resistance and inductivity respectively. With the above notations the total impedance can be written in frequency domain, as follows:

$$Z_0(j\omega) = R_e + L_e \cdot j\omega + \frac{j\omega}{C_m \cdot (j\omega)^2 + R_m^{-1} \cdot j\omega + L_m^{-1}} = Z_{0e}(j\omega) + Z_{0m}(j\omega) \quad (3)$$

Equation3 represents the total impedance of the actuator itself. It has two components. $Z_{0e}(j\omega)$is the so called blocked impedance, which depends only on the electrical parts, R_e and L_e. It can be measured directly with a RLC bridge by blocking the movement of the coil from outside. $Z_{0m}(j\omega)$is represents the so called motional impedance that is related mostly to mechanical parts. Nevertheless, it includes also the influence of the electrical part by means of the induced voltage in the coil due to its speed. Moreover, if the load impedanceZ_L,is also taken into account, the new impedance becomes:

$$Z_0 = Z_{0e}(j\omega) + \frac{Z_{0m}(j\omega) \cdot Z_L(j\omega)}{Z_{0m}(j\omega) + Z_L(j\omega)} \quad (4)$$

which is calculated by means of parallel connection of motional impedance with the load impedance. There is a lack of knowledge to develop a proper model of the load impedance and therefore, the load influence on the overall behaviour can be considered as disturbance. Therewith, a control scheme with good ability to overcome the effects of disturbances is required.

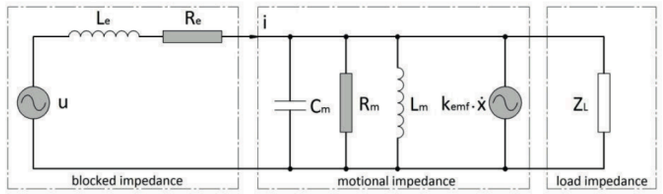

Figure 2: Actuator impedance model

In case of a voice coil driven servo valve, some parameters, which would describe the load impedance, can be included in motional impedance. One of these is the spool's mass, which can be added to the coil assembly mass, increasing therefore the mechanical capacity. The damping behaviour is related to the friction between the spool and the sleeve due to the fluid viscosity. This behaviour can also be taken into account by means of the overall damping coefficient,c_D.Some parameters can be estimated with sufficient accuracy by measurements, like coil DC resistance at a given temperature, coil inductance, the total movable mass and the spring stiffness. The estimation of other parameters, like the damping coefficients, can be more difficult and requires ,e.g, to perform flow simulations (CFD) of the valve's behaviour under certain conditions. A simple way to estimate the damping of a given servo valve will be presented later in this paper.

4 The control strategies

The developed force of the voice coil motor is directly related to the current that flows troughs the coil windings. Therefore, a very good transient behaviour of the current control system is required, especially when high transient flow forces are developed, e.g., as a result of a fast transition at small openings of a servo valve's spool.

4.1 The speed feedback

One of the most significant issues of voice coil motors is the relatively small damping /8/. Near the resonant frequency of the coil assembly, the total impedance, seen by the voltage supply, raises quickly and reaches a maximum value, which is sometimes an order higher, relative to the impedance at low frequencies. The increasing impedance effectively blocks the current to flow through the coil windings and the motion of the coil assembly gets out of control.

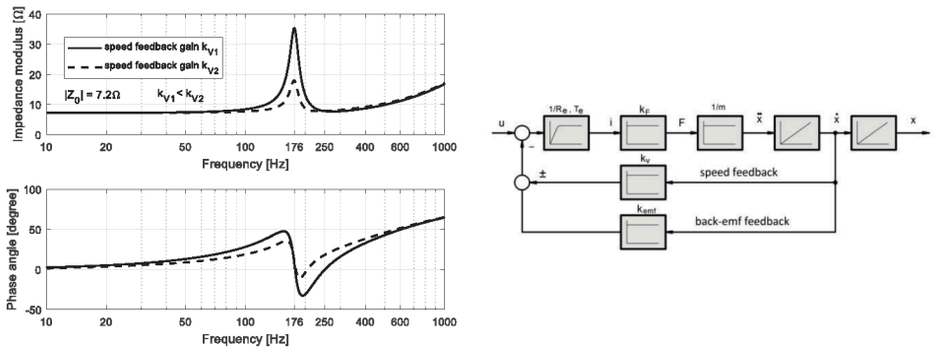

Figure 3: The influence of the speed feedback on the equivalent electrical impedance

The well-known speed feedback is used to improve the damping behaviour, but there are some limitations. In order to be effective, this feedback strategy must fulfil some conditions and namely the bandwidth of the electrical part must be much higher than the bandwidth of the mechanical part /9/. With the given parameters of the developed prototype $\tau_e = 0.388$ ms, the -3dB corner frequency of the electrical part (blocked impedance) lies at a frequency higher than 2000 Hz, which is much higher than the mechanical natural frequency$\omega_m =$ 176 Hz. There are also limits to increase the k_v gain, by means that the feedback voltage cannot be higher than the voltage supply.Mathematically, the speed feedback will be done by adding or subtracting the speed gain,k_V, to or from the back-emf constant, as shown in figure 3, right. By this, the virtual electric parameters become:

$$C_m = \frac{m}{k_F \cdot (k_{emf} \pm k_v)}, R_m = \frac{k_F \cdot (k_{emf} \pm k_v)}{c_D}, L_m = \frac{k_F \cdot (k_{emf} \pm k_v)}{k_E} \quad (5)$$

As it is shown in figure 3, the speed feedback operates just on the impedance at the resonant frequency, thus reducing the impedance peak and doesn't affect the impedance at low frequencies. According to equation 3, the total impedance at $\omega = 0$ is:

$$|Z_0(j\omega)|_{\omega=0} = R_e \tag{6}$$

At the resonant frequency$\omega = \omega_{0m}$the total impedance becomes:

$$|Z_0(j\omega)|_{\omega=\omega_{0m}} = |R_e + L_e \cdot j\omega_{0m} + R_m| = \left|R_e + L_e \cdot j\omega_{0m} + \frac{k_F \cdot (k_{emf} \pm k_v)}{c_D}\right| \tag{7}$$

which can be adjusted by changing the speed gain.

4.2 PID control

Due to its simple design and performance characteristics a PID controller has been used first in the closed loop control of the actuator prototype. One of the main drawbacks of the PID controller arises from the fact that the control action takes place without a comprehensive knowledge of the process dynamics. Although some good performances were achieved, the overall stationary and transient behaviour was a compromise between a higher dynamics and a well damped system.

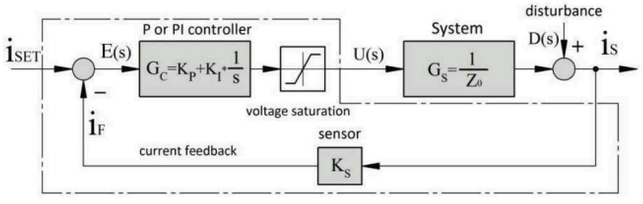

Figure 4: PI control of the current system

The PID control of the prototype was implemented according to the scheme in figure 4. Additional information on PID control and its properties can be found in /16/, /17/. However, to have a comparative basis, the step responses in current and position, determined during the experimental phase of the prototype development are presented in figure 5 /8/.

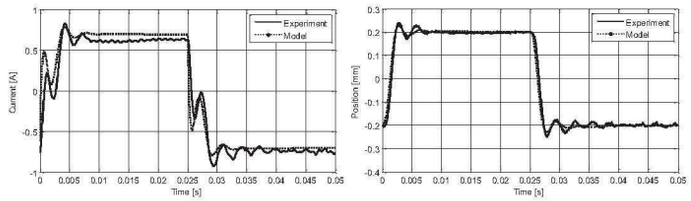

Figure5: Step responses in current and position /8/

The current behaviour (figure 5,left) shows a relatively large oscillation during the transient phase, as well a relatively large overshoot as the current approaches the steady-state value. However, a good agreement between the experimental and simulation results can be observed. This similarity will be useful in the design of the following control strategy, based on the internal model control.

4.3 Internal model control (IMC)

The internal model control principle /16/, /17/, /18/, /19/ is based, first of all, on a comprehensive knowledge of the system model. To achieve certain robustness the controller must include a low pass filter. Its order has to be adjusted to the model order. The filter must be selected in such way that the controller is physically realisable. This implies that the transfer function $G_C^* = G_C(s) \cdot G_F(s)$ must be proper, otherwise excessive derivative action occurs. Here G_C is the transfer function of the controller and $G_F$the transfer function of the filter.

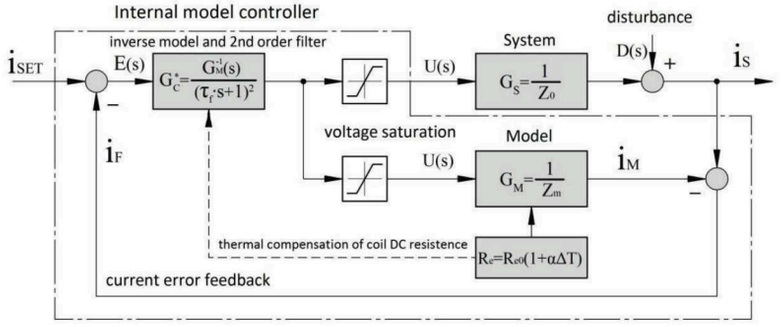

Figure 6: The implementation of the internal model control IMC.

Some properties of the IMC control are /16/, /17/, /19/:

- Dual stability - if the model perfectly matches the system and if the system and controller are both stable, the IMC structure guarantees the closed loop stability;
- Supposing that the controller transfer function is exactly the inverse of the model transfer function, than there is no steady-state error at the output for both inputs, set point and disturbance.

The structure of the internal model control (IMC), figure 6, uses a feedback signal, i_F, built as the difference between the system output,i_S and the model output, i_M. If the model $G_M(s)$ perfectly matches the system $G_S(s)$ then the feedback signal $i_F(s)$ represents the disturbance $D(s)$. Also, if the disturbance $D(s) = 0$, then the signal $i_F$is a measure of the discrepancies between the system and the model. The signal i_F is then subtracted from the set point i_{SET} resulting in the input signal of the controller, E. The voltage at the controller's output is feed into both, the real system and its model. This voltage forces the system to behave like the model. One of the most important properties of the IMC is the ability to efficiently reject the effects of disturbances. This behaviour takes place even if there are some discrepancies between the system and the model.

In the following the transfer function of the closed loop system is calculated according to the IMC control structure, shown in figure 6. To simplify the notations the complex variable s is omitted. So, for example $G_C$means $G_C(s)$. Referring to figure 6, the signal $I_S$equals:

$$I_S = G_C \cdot G_S \cdot E + D \tag{8}$$

and the output of the model is:

$$I_M = G_C \cdot G_M \cdot E \tag{9}$$

The controller's input is defined by:

$$E = I_{SET} - I_F = I_{SET} - (I_S - I_M) = I_{SET} - E \cdot G_C \cdot (G_S - G_M) - D \tag{10}$$

or

$$E = \frac{I_{SET} - D}{1 + G_C \cdot (G_S - G_M)} \tag{11}$$

The output of the system is:

$$I_S = \frac{I_{SET} \cdot G_C \cdot G_S + (1 - G_C \cdot G_M) \cdot D}{1 + G_C \cdot (G_S - G_M)} \tag{12}$$

Now, if the transfer function of the controller,G_C, is exactly the inverse of the model transfer function G_M, that is:

$$G_C = G_M^{-1} \tag{13}$$

the disturbance D is completely rejected, even if there are some differences between the real system $G_S(s)$ and his model$G_M(s)$. The output of the real system is then:

$$I_S = \frac{I_{SET} \cdot G_C \cdot G_S}{1 + G_C \cdot (G_S - G_M)} \tag{14}$$

Moreover if the model $G_M(s)$ exactly matches the real system $G_S(s)$, then:

$$I_S = \frac{I_{SET} \cdot G_C \cdot G_S}{1 + G_C \cdot (G_S - G_M)} = \frac{I_{SET} \cdot G_M^{-1} \cdot G_M}{1 + G_M^{-1} \cdot (G_M - G_M)} = I_{SET} \tag{15}$$

and therefore the output current of the real system perfectly follows the input.

The transfer function of the system is calculated by taking the inverse of the total impedance $Z_0(j\omega)$ and replacing the variable $j\omega$ with the complex variable s:

$$G_S(s) = \frac{1}{Z_0(s)} = \frac{C_\mathrm{m} \cdot s^2 + \frac{1}{R_\mathrm{m}} \cdot s + \frac{1}{L_\mathrm{m}}}{L_\mathrm{e} C_\mathrm{m} \cdot s^3 + \left(R_\mathrm{e} C_\mathrm{m} + \frac{L_\mathrm{e}}{R_\mathrm{m}}\right) \cdot s^2 + \left(\frac{R_e}{R_\mathrm{m}} + \frac{L_e}{L_\mathrm{m}} + 1\right) \cdot s + \frac{R_\mathrm{e}}{L_\mathrm{m}}} \tag{16}$$

The transfer function of the model takes the same form, but the coefficients are in this case estimates of the system coefficients:

$$G_M(s) = \frac{1}{Z_M(s)} = \frac{C_\mathrm{m}^* \cdot s^2 + \frac{1}{R_\mathrm{m}^*} \cdot s + \frac{1}{L_\mathrm{m}^*}}{L_\mathrm{e}^* C_\mathrm{m}^* \cdot s^3 + \left(R_\mathrm{e}^* C_\mathrm{m}^* + \frac{L_\mathrm{e}^*}{R_\mathrm{m}^*}\right) \cdot s^2 + \left(\frac{R_\mathrm{e}^*}{R_\mathrm{m}^*} + \frac{L_\mathrm{e}^*}{L_\mathrm{m}^*} + 1\right) \cdot s + \frac{R_\mathrm{e}^*}{L_\mathrm{m}^*}} \tag{17}$$

The transfer function of the controller results of a series connection of the model impedance with a low pass filter:

$$G_C^*(s) = \frac{G_M^{-1}(s)}{(\tau_\mathrm{f} \cdot s + 1)^2} = \frac{Z_M(s)}{(\tau_\mathrm{f} \cdot s + 1)^2} \tag{18}$$

The filter time constant is the only tuning parameter of the controller, making the tuning process much easier. A low value of the time constant leads to a smoother response but also a lower bandwidth. A high value, however, leads to a noisy system, especially in case there are some significantly discrepancies between system and model or in case of model uncertainties.

5 The simulation models and simulation results

5.1 Estimating the damping coefficient of a real servo valve

In order to estimate the damping coefficient of a real valve, some parameters must be taken into account. The damping coefficient depends on a number of factors like viscosity, temperature, the clearance between the spool and the sleeve, the number and the length of the spool's shoulders. Some authors have proposed the following formula to calculate the damping coefficient /14/, /15/:

$$c_\mathrm{D} = \eta \cdot n \cdot l_\mathrm{s} \cdot R_0 = \nu \cdot \rho \cdot n \cdot l_\mathrm{s} \cdot R_0 \tag{19}$$

where the equivalent radius is:

$$R_0 = \frac{8\pi \cdot (R_2^2 - R_1^2)}{R_2^2 + R_1^2 - \frac{R_2^2 - R_1^2}{ln(R_2/R_1)}} \tag{20}$$

withR_1 the spool radius and $R_2$the sleeve radius respectively.

Property	Density	Viscosity at $+40^oC$	Viscosity at $+100^oC$
Value	0.880	46	6.7
Units	$[g/cm^3]$	$[mm^2/s]$	$[mm^2/s]$

Table 2: Some properties of hydraulic oil HLP46 according to DIN51524 specifications (LIQUIMOLY)

For a nominal size NG10 of a given servo valve, the spool diameter is $D_1 = 2 \cdot R_1 = 9.992\ mm$and the sleeve diameter is $D_2 = 2 \cdot R_2 = 10.000\ mm$. The spool has four shoulders, each having a length of $l_s = 6\ mm$. With the values of the parameters given in table 2, the calculated damping coefficients for 40°C and 100 °C are $c_{D40} = 91.5\ N \cdot s/m$ and $c_{D100} = 13.3\ N \cdot s/m$. respectively.

5.2 The impedance of the system under control

The total system impedance can be calculated by taking the inverse of the transfer function given by equations16 (system) and 17 (model). A Matlab code was written to calculate the overall impedance as a function of the frequency and to represent the corresponding curves.

The impedance curve of the system under IMC control, shown in figure 7 with dashed line, corresponds to the ideal case, as the transfer function of the model perfectly matches the transfer function of the system. A smooth change in phase can be observed and a 90^o phase shift, between the current and applied voltage, occurs at a frequency above 1000 Hz. The IMC control theoretically allows the overall system to behave like a pure resistive impedance of 1Ω, at the frequencies lower than the low pass filter corner frequency $f = 1/\tau_\mathrm{f}$.The PI control (dotted line), allows to reduce the overall impedance to a value of about 4Ω,for frequencies lower than resonant frequency, as well as the peak resonance to a value lower than 10Ω.

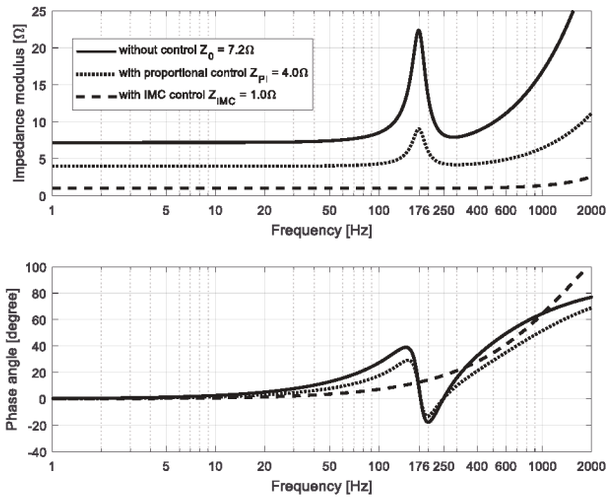

Figure 7: Comparison between impedance curves using different control strategies

The Bode plot in figure 8 shows the frequency behaviour of the system for three cases. The represented curves correspond to the open loop behaviour (dotted line), closed loop with PI control (dashed line) and closed loop with IMC control (continuous line) respectively. In all three cases the speed feedback was switched on.

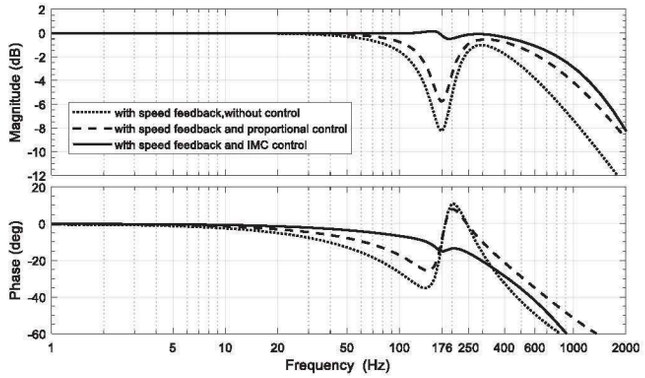

Figure 8: Current dynamics - Bode plot

To highlight the effect of a system-model mismatch, an overestimated damping coefficient was taken into account for the model ($c_D = 20$and $c_D^* = 35$). The corresponding behaviour can be observed around the resonant frequency (176 Hz). The -3dB frequency lies at a frequency of about 1000 Hz in case of IMC control with a smooth behaviour along the frequency.

5.3 Stability of the system under IMC control

To verify the stability of the controlled system both the transfer function of the system $G_S(s)$, as well as the transfer function of the controller $G_C^*(s)$, were converted in a state-space representation /16/.

$$\begin{cases} \dot{x} = A \cdot x + B \cdot u \\ y = C \cdot x + D \cdot u \end{cases} \tag{21}$$

with x, the vector of state variables, A, the state matrix, B, the input matrix, u, the vector of the input signals, y, the vector of the output signals, C, the output matrix, and$D$, the feed forward matrix. Next,the eigenvalues of the state matrix A for both the system and the controller is calculated. Using dedicated Matlab code /20/, with dedicated function and using the numerical values given in table 1 and $\tau_f = 0.1$ms, the eigenvalues are:

$$eig(A_S) = 10^3 \cdot [-2.39 \quad -0.39 + 1.15 \cdot i \quad -0.39 - 1.15 \cdot i] \tag{22}$$

with A_S being the system state matrix and

$$eig(A_{C^*}) = 10^3 \cdot [-10 + 6.02 \cdot 10^{-8} \cdot i \quad -10 - 6.02 \cdot 10^{-8} \cdot i - 0.25 + 1.8 \cdot i \quad -0.25 - 1.8 \cdot i] \tag{23}$$

with A_{C^*} being the controller state matrix. All real part of the state matrix eigenvalues are negative, thus both the system and the controller are stable. Based on the property of the IMC structure, if both the system and the controller are stable and the model matches the system, the closed loop is stable as well.

5.4 The Simulink simulation model

The Matlab-Simulink model /20/, includes both types of control (PI and IMC) to allow the comparison of step responses for the same set point, as well as for the same disturbances. Both models include also the speed feedback already described. The simulation model was driven first by an input signal of 2A (figure 10), at the simulation time $t = 5ms$ and the system was loaded with a disturbance signal of -1.5 A (at time $t = 20ms$), which represents 75% of the input signal (heavy load).

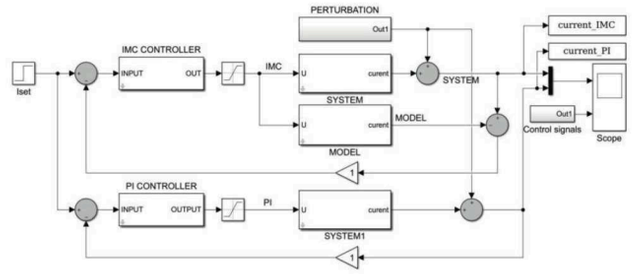

Figure 9: The simulation model - Simulink

A fast, smooth and also overshoot free response can be observed in case of IMC control, thus proving its robustness. The disturbance is also fast and smooth rejected.

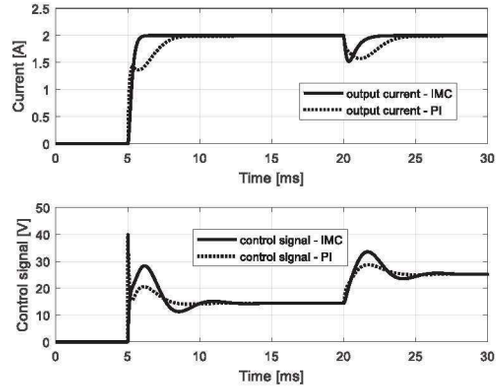

Figure 10: Comparison between step responses with two controller types

In contrast, the system response under PI control takes more as double the time to approach the steady state value, for both the input as well as the disturbance signal. Moreover, the response shows a slight undershoot.

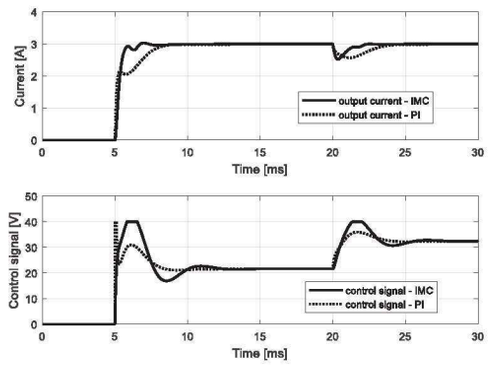

Figure 11: The effect of the voltage limitation at higher set point currents (3A)

Appropriate saturation blocks were introduced in the simulation model to simulate the voltage limitation of the controller. The limits were set to ±40V. As it has been shown in figure 10, a higher voltage reserve from the power supply can be observed in case of IMC control (about 10V for 2A current set point). In comparison, the control signal in case of PI control goes already in saturation. In the next test case, the model was driven by a higher input signal of 3A, as shown in figure 11, and the disturbance signal was maintained at the same level as

above. The control signal goes in saturation for both models. The IMC response takes longer time to approach the steady state, but is obviously faster than PI response and shows a slight undershoot. As a recommendation, a higher voltage supply than nominal voltage of the voice coil motor is required (usually 50% higher) in order to ensure a faster transient phase, a smoother response and a good ability to overcome the effect of disturbances, especially in case of higher input signals, as well as in case of high level of disturbances.

6 Summary and Conclusion

The paper deals with a comparative study of different control strategy types, applied to overcome the increase in impedance of voice coil motors at resonance frequency and its effects on the overall transient behaviour. The speed feedback, proportional-integral control (PI) and internal model control (IMC) strategies are presented and discussed. The proposed models were investigated and interpreted using the electrical analogy. Several improvements are shown and implemented in simulation models in order to stabilise and to lower the impedance over a wide range of frequencies, thus increasing the bandwidth. The numerical values of the parameters used in simulation, correspond to a prototype already developed by the authors. Finally, simulation results are presented and discussed. The future work will be focused on experimental research to verify and test the model validity and to make appropriate adjustments, in order to achieve better performances. The development of an accurate load impedance model, corresponding to a real valve and the investigation of its influence on the actuator-valve assembly are also future objectives.

7 Acknowledgements

Part of this work was supported by the German Academic Exchange Service (DAAD) and the Institute for Fluid Power Drives and Systems at RWTH Aachen University (IFAS).

Nomenclature

Variable	*Description*	*Unit*	*Variable*	*Description*	*Unit*
u	Coil supply voltage	[V]	i	Coil current	[A]
R_e	Coil DC resistance	[Ω]	L_e	Coil total inductance	[H]
m	mass of coil assembly	[Kg]	x	Coil position	[m]
k_{emf}	Back-emf constant	[V s/m]	k_F	Motor force factor	[N/A]
k_E	Suspension stiffness	[N/m]	c_D	Damping coefficient	[N s/m]

References

/1/ Reichert, M., *Development of High-Response Piezo-Servovalves for Improved Performances of Electrohydraulic Cylinder Drives,* Thesis RWTH Aachen University, Shaker, Aachen, Germany, 2010.

/2/ *Direct Operated Proportional DC Valve Series D1FP*, www.parker.com, 2017.

/3/ Ruggeri, M., Marani, P., *A New High Performance Roto-Translating Valve for Fault Tolerant Applications*, SAE Technical Paper 2014-01-2403, 2014.

/4/ Ruggeri, M., Marani, P., *New Roto-Translating Valve Functional and Safety Feature Analysis*, 9th JFPS International Symposium on Fluid Power, Matsue, Japan, 2017.

/5/ Roemer, D.B., Bech, M.M., Johansen, P., Pedersen, H.C., *Optimum Design of a Moving Coil Actuator for Fast-Switching Valves in Digital Hydraulic Pumps and Motors*, IEEE/ASME Transactions on Mechatronics Volume 20, Issue 6, December 2015, Article number 7084166, Pages 2761-2770.

/6/ Guo, H., Wang, D., Xu, J., *Research on a high-frequency response direct drive valve system based on voice coil motor*, IEEE Transactions on Power Electronics, Volume 28, Issue 5, Article number 6313926, Pages 2483-2492, 2013.

/7/ Wu, S., Jiao, Z., Yan, L., Zhang, R., Yu, J., Chen, C.-Y., *Development of a direct-drive servo valve with high-frequency voice coil motor and advanced digital controller*, IEEE/ASME Transactions on Mechatronics Volume 19, Issue 3, Article number 6523134, Pages 932-942, 2014.

/8/ Nascutiu, L., Reinertz, O., Siebert, C., Murrenhoff, H., High Performance Actuators for Fluid Power Drives, The 9th International Fluid Power Conference, vol. 3., Aachen, Germany; 03/2014.

/9/ Nascutiu, L., *Voice Coil Actuator for Hydraulic Servo Valves with High Transient Performances*, Automation, Quality and Testing, Robotics, 2006 IEEE International Conference, Cluj-Napoca, Romania, pp. 185 – 190, May 25-28, 2006.

/10/ Schmitz, J.,Vatheuer, N., Murrenhoff, H., *Hydrostatic Transmissions: A Power Play in Wind Turbine Design*, Hydraulics & Pneumatics, 2013.

/11/ Anton, I., Vekas, L., *Brochure Magnetic Fluids – a special category of nanomaterials, proprieties and applications*, Romanian Academy –Timisoara Branch and "Politehnica" University Timisoara, 2002.

/12/ Schurer, H., *Linearization of Electroacoustic Transducers*, Thesis University of Twente Enschede, ISBN 90-365-1032-5, Print Partners Ipskamp, Enschede, Netherlands, 1997.

/13/ Thorborg, K., Unruh, A., Struck, C., *An Improved Electrical Equivalent Circuit Model for Dynamic Moving Coil Transducers*, Audio Engineering Society, Convention Paper presented at the 122th Convention, Vienna, Austria, May 5-8, 2007.

/14/ Deacu, L., Banabic, D., Radulescu, M., Ratiu, C., *Tehnica Hidraulicii Proportionale,* Dacia, Cluj-Napoca, 1989.

/15/ Lescenko, V.A., *Ghidravliceskie slediascie privodî stankov s programnîm upravleniem,* Mașinostroenie, Moskva, 1975.

/16/ Levine, W. S., *The Control Handbook, Second Edition: Control System Fundamentals*, CRC Press, 2010.

/17/ Levine, W. S., *The Control Systems Handbook, Second Edition: Control System Advanced Methods*, CRC Press, 2010.

/18/ Tham, M. T., *Internal Model Control*, Chemical and Process Engineering, University of Newcastle upon Tyne, 2002.

/19/ Muhammad, D., Ahmad, Z., Aziz, N., *Implementation Of Internal Model Control (IMC) In Continuous Distillation Column*, The 5th International Symposium on Design, Operation and Control of Chemical Processes, PSE ASIA 2010, Singapore, July 25-28, 2010.

/20/ *** www.mathworks.com, *Control system toolbox*